A Generalized Scattering Matrix Approach for Analysis of Quasi-Optical Grids and De-Embedding of Device Parameters

Larry W. Epp, *Member, IEEE*, and R. Peter Smith, *Member, IEEE*

Abstract— **A generalized scattering matrix approach to analyzing quasi-optical grids used for grid amplifiers and grid oscillators is developed. The approach is verified by a novel method for de-embedding, in a waveguide simulator, the active device parameters of a differential pair high electron mobility transistor (HEMT) from the single unit cell of a grid amplifier. The method incorporates the additional ports presented to the active device into a method of moments solution of the embedding periodic array. The port(s) defined at the device or load location are within the plane of the array, and not terminated in a microstrip line with a known characteristic impedance. Therefore the generalized scattering matrix for the embedding array is normalized to the calculated input impedance(s) at these port(s). The approach described here uses a Floquet representation of the fields incident and reflected from the grid as the remaining ports in the generalized scattering matrix. The use of Floquet modes allows analysis of general geometries and nonnormal incident angles without the need for magnetic and electric wall assumptions. By developing a generalized scattering matrix for the embedding periodic array, this approach now allows conventional amplifier design techniques and analysis methods to be applied to quasi-optical grid amplifier and oscillator design. The major advantage of this unification for grid amplifier design being that the stability of the design can be predicted.**

I. Introduction

In a simple, single layer grid oscillator or grid amplifier design, a large number of solid state devices are combined in a periodic array, or grid, that is supported by a dielectric substrate layer. This provides a means for spatial power combining in the cases of grid oscillators, and spatial amplification in the case of grid amplifiers, making these approaches attractive for quasi-optical systems. In designing these systems, what is needed is a design and analysis method that combines: 1) the quasi-optical nature of the exciting electromagnetic fields, 2) the periodic nature of the array, and 3) the solid state device parameters which are often given in the familiar S parameter form.

The basis for this design philosophy has its beginnings in the equivalent circuit approach [1], that separates the equivalent circuit of the grid or array, from the model for the device. This equivalent circuit approach allows the device parameters to be included into a model of a single unit cell of the grid. Equivalent circuit approaches are limited by the accuracy of the assumed current distributions, which allow for the placement of electric and magnetic walls in the unit cell. But the relative simplicity of the approach has allowed it to be applied successfully to both oscillators [2], [3] and grid amplifiers [4], [5].

To allow for a more general representation of the unit cell, a more detailed analysis using a current discretization on the unit cell has been done recently by Bundy *et al.* [6], [7]. Their approach elevates the design procedure to one which finds the scattering matrix for the periodically repeated grid unit cell, what will be referred to here as the embedding array, and one for the scattering matrix of the device. Unfortunately, magnetic and electric walls are still needed, and therefore only a single TEM input polarization can be used. What is needed is an analogous approach to multimode networks of planar periodic gratings [8], that uses a complete set of fields to generate a scattering matrix for the embedding array. The complete set of fields must be valid for normal and nonnormal excitation, and include the two orthogonal input and output polarizations. Thus the method described here combines a generalized scattering matrix representation for the fields scattered from a periodic grid [9], [10], with the the port locations for the device [11], and finally with the scattering matrix representation for the device.

Since a common configuration for grid amplifiers is one that uses two orthogonal polarizations for input and output [4], the two orthogonal polarizations will be included in the generalized scattering matrix developed here. Thus for angles including normal incidence, the orthogonal polarizations will be described by the TE and TM decompositions of the Floquet harmonics, which are determined by the periodicity of the grid cells. This allows the effects of coupling between the input and output ports shown in Fig. 1, aggravated by the presence of the dc bias lines needed for device biasing, to be included in the analysis. The coupling between input and output ports is a critical parameter in determining stability of a grid amplifier design in order to avoid unwanted oscillations. Potential instabilities of the system can be examined when the generalized scattering matrix developed here is combined with the scattering matrix of the device.

Manuscript received September 14, 1995; revised January 17, 1996. This work was performed at the Jet Propulsion Laboratory, California Institute of Technology under a contract with the National Aeronautics and Space Administration. Device fabrication work was performed at the Center for Space Microelectronics Technology, Jet Propulsion Laboratory, California Institute of Technology, and was sponsored by the Innovative Science and Technology Office of BMDO through an agreement with NASA.

The authors are with the Jet Propulsion Laboratory, California Institute of Technology, Pasadena, CA 91109 USA.

Publisher Item Identifier S 0018-9480(96)03029-3.

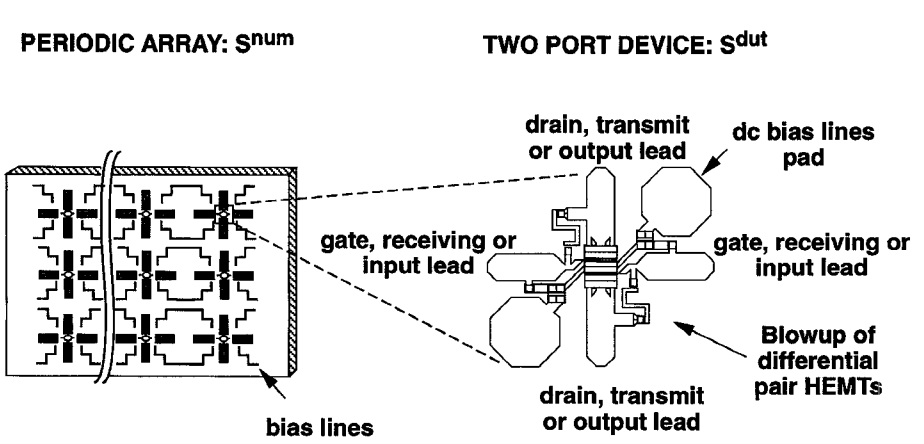

Fig. 1. Overview showing distinction between the generalized scattering matrix of the grid, S^{num}, and the differential pair device under test. Note that input and output are separated by orthogonal polarizations at normal incidence.

One of the key future prospects of grid amplifier/oscillator technology is the desire to monolithically fabricate the entire amplifying array on a single wafer for high frequency applications. This would avoid hybrid approaches, leading to more consistent device placement, connection, and consistency among device characteristics. This in turn, would allow for maximum reliability and performance of the grid while minimizing cost. In order to simplify the fabrication, it is desirable that the array be planar in nature, with the need for via holes kept to a minimum. In doing this, as in [4], the amplifying device is not placed within an unbalanced microstrip line configuration but in balanced differential mode. This makes it difficult to measure device S parameters in the array environment, or using conventional 50 Ω microstrip line measurement techniques. But once the generalized scattering matrix approach as described here is applied, the planar array is described by a known scattering matrix which then becomes the embedding network [12]. Once known, the scattering parameters of the embedding network, the embedding array, can be used to de-embed the amplifying device parameters. This approach will be used to de-embed the S parameters of a differential pair HEMT using a single unit cell in a waveguide simulation of the infinite array. Note that the S parameters of the differential pair HEMT will be referred to as S^{dut}, as it is the device under test.

II. Generalized Scattering Matrix with Device Ports

Fig. 1 shows the general geometry of the grid amplifier that is to be modeled. Input and output antennas are shown as orthogonal dipoles, with the horizontal dipole providing a port location to which the gates of the differential pair HEMT are attached, and the vertical dipole providing the output port at which the drains of the device are connected. In order to form a complete set for the field components on both sides of the grid amplifier, they are described by Floquet harmonics as shown in Fig. 2. Note that the grid amplifier is described by Floquet harmonics in the two half-spaces designated regions 1 and 2, where the z axis forms the normal to the embedding array. As depicted in Figs. 1 and 2, the purpose of the method proposed is to find the generalized scattering matrix that describes the periodic array containing the two device ports, S^{num}. The array is assumed to be infinite and periodic in the plane perpendicular to the z axis, so that a single unit cell of the structure can be modeled. Note that S^{num} represents the scattering matrix of the embedding periodic array, and does not include the scattering matrix of the device(s) S^{dut}.

To find S^{num}, the unit cell is described in terms of the currents on the metallic surfaces of the unit cell, including those of any bias lines present. These currents will generate scattered fields in terms of Floquet harmonics, where each scattered Floquet harmonic represents a port in the generalized scattering matrix to be computed. To find the scattering matrix, S^{num}, the structure is excited with an incident Floquet Harmonic at one port, and the coefficients of the scattered harmonics in region 1 and region 2 are computed with all ports matched. Since the infinite half spaces are inherently matched, it is necessary to match the ports at the device locations. This is done by first computing the input impedance at each of these ports, which is used as the reference impedance for these port locations. The scattering parameters between the incident Floquet harmonic ports and all the other ports, including device ports, are then found directly. The scattering parameters between device ports and Floquet harmonics are then computed from the symmetry of the generalized scattering parameters.

A. Scattered Fields

To find the scattered Floquet modes at the output ports 1 to $n+m$ in Fig. 2, it is necessary to compute the scattered fields from the periodic array when all ports are matched. The scattered and incident fields can be related to the surface currents by enforcing the electric field boundary condition on the metallic surfaces of the unit cell using the impedance boundary condition [13]

$$\vec{E}^{\text{inc}} + \vec{E}^{\text{scat}} = \vec{Z}_s \vec{J}_s. \tag{1}$$

Here Z_s account for surface losses, and will later be generalized to include the port locations, loaded in their terminating impedances, needed for the active device.

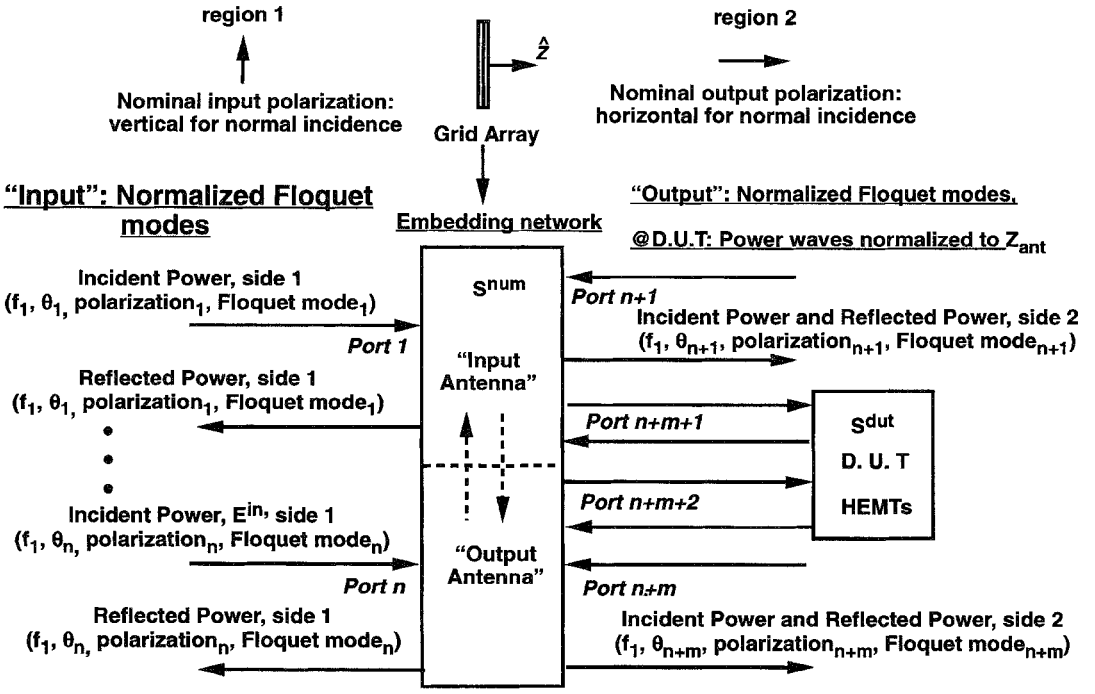

Fig. 2. General form of generalized scattering matrix containing $n + m$ Floquet modes in region 1 and region 2.

Formulating with the spectral domains Green's functions as done by Tsao [14]

$$\begin{bmatrix} E_x^{\text{inc}}(x,y,0) \\ E_y^{\text{inc}}(x,y,0) \end{bmatrix} = \sum_{m,n=-\infty}^{m,n=+\infty} \begin{bmatrix} \tilde{G}_{xx}(m,n) & \tilde{G}_{xy}(m,n) \\ \tilde{G}_{yx}(m,n) & \tilde{G}_{yy}(m,n) \end{bmatrix} \cdot \begin{bmatrix} \tilde{J}_x(m,n) \\ \tilde{J}_y(m,n) \end{bmatrix} \Psi(m,n) - Z_s \begin{bmatrix} J_x \\ J_y \end{bmatrix}. \quad (2)$$

Note that the Green's functions $\tilde{G}$ are modified according to the spectral domain immitance [15] approach to contain the effects of the superstrate and substrate layers supporting the metallic layer. And, that the Floquet harmonics

$$\Psi(m,n) = e^{jk_{xm}x + jk_{yn}y \mp \gamma_{mn}z} \quad (3)$$

$$k_{xm} = \frac{2\pi m}{T_x} + k_x^{\text{inc}},$$

$$k_{yn} = \frac{2\pi n}{T_y} + k_y^{\text{inc}}, \quad \text{and}$$

$$\gamma_{mn} = \sqrt{k_o^2 - k_{xm}^2 - k_{yn}^2} \quad (4)$$

are related to the unit cell dimensions and the propagation constants of the incident field. Here T_x is the dimension of the unit cell in the x-direction and k_x^{inc} is the corresponding phase shift of the incident field due to nonnormal incidence. The unit cell dimension in the y-direction is T_y and phase shift k_y^{inc} is defined accordingly.

Next the unit cell is divided into an M by N grid of rectangular subdomains that are spanned by rooftop basis functions. By appropriately choosing $M = N = 2^n$ the unit cell is discretized in a manner such that one can take full advantage of the fast Fourier transform method to speed up the numerical evaluation of the integrals involved [16]. Extending the surface impedance so that it is a function of position leads to a surface impedance that can be specified on each individual patch in the M by N grid [17]. Once this is done, the ports for the device under test can be matched by specifying the surface impedance at the port location such that the current and voltage at the port are related by the terminating impedance. Using Galerkin's method, a solution for the currents then allows for the computation of the scattered fields in terms of Floquet harmonics reflected and transmitted by the grid. The currents also allow the power absorbed at the device locations to be computed under matched conditions, and thus the scattering parameters at these ports. These will be discussed in the next sections.

B. Normalized Floquet Modes

The analogous voltages and currents of the Floquet harmonics must be computed in order to properly normalize the scattering parameters of the periodic grid and ensure that a symmetric scattering matrix results. Since the quantities of interest are the scattered fields themselves, the Floquet modes for the tangential electric fields are [18]

$$\vec{e}_{\text{TE}}^{\pm}(m,n) = \sqrt{\frac{j\omega\mu_o}{\gamma_{mn}}} \frac{1}{\sqrt{\text{cell area}}} \cdot \frac{1}{\sqrt{k_o^2 + \gamma_{mn}^2}} (-k_y \vec{x} + k_x \vec{y}) \Psi(m,n) \quad (5)$$

$$\vec{e}_{TE}^{\pm}(m,n) = \sqrt{\frac{\gamma_{mn}}{j\omega\epsilon}} \frac{1}{\sqrt{\text{cell area}}} \cdot \frac{1}{\sqrt{k_o^2 + \gamma_{mn}^2}} (k_x \vec{x} + k_y \vec{y}) \Psi(m,n) \quad (6)$$

where $\pm$ indicates that the sign of the electric field components remains the same for propagation in the $+z$ or $-z$ directions.

The tangential magnetic fields can be found through the characteristic impedance

$$\vec{e}_i(m,n) = \mp Z_i \vec{z} \times \vec{h}_i(m,n) \begin{cases} -\text{for } (+z) \text{ propogation} \\ +\text{for } (-z) \text{ propagation} \end{cases} \quad (7)$$

where i is either TE or TM and

$$Z_{\text{TE}} = \frac{j\omega\mu_o}{\gamma_{mn}}, \quad Z_{\text{TM}} = \frac{\gamma_{mn}}{j\omega\epsilon}. \quad (8)$$

The tangential fields are sufficient to define the normalized Floquet voltage waves [9] at a plane z as they represent power traveling in the $\pm z$ direction. Note that in defining the TE and TM fields, such as shown in (5) and (6), they have been normalized to obtain a symmetric scattering matrix for reciprocal structures

$$\iint_{\text{unit cell}} \vec{e}_i^{\pm} \times \vec{h}_i^{\pm} \cdot (\pm\vec{z})\, dS = 1, \qquad i = \text{TE or TM}. \quad (9)$$

The normalizing direction, $\pm\vec{z}$, is dependent on whether the waves are forward or backward traveling. Therefore the sign of either $\vec{e}_{\text{TE}}$ or $\vec{h}_{\text{TE}}$ must change dependent on the direction of propagation. As mentioned previously, it is convenient to choose the sign of the electric field components to remain the same, except for the necessary change on the γ_{mn} exponent in (4). Thus

$$\vec{e}_i^{+} = \vec{e}_i^{-} \quad \text{and} \quad \vec{h}_i^{+} = -\vec{h}_i^{-} \quad \text{for } z = 0, \quad i = \text{TE or TM} \quad (10)$$

guarantees that reflection from a pec plate will give a reflection coefficient of -1.

The total tangential electric field at a reference plane $z = z'$ is then weighted by the appropriate coefficients of the normalized Floquet harmonics

$$\vec{E}_i(m,n) = C_i^{+}(m,n)\, \vec{e}_i^{+}(m,n) + C_i^{-}(m,n)\vec{e}_i^{-}(m,n) \qquad i = \text{TE or TM} \quad (11)$$

where $C_{\text{TE}}^{+}(m,n)\ \vec{e}_{\text{TE}}^{+}(m,n)$ is analogous to the forward traveling voltage on a transmission line. Likewise the magnetic field will correspond to the forward traveling current, which is related to the electric field via (7). From (11) the scattering parameters can be defined at port i due to an incident Floquet harmonic at port j,

$$S_{ij} = \frac{C_i^{\pm}(m,n)\ \vec{e}_i^{\pm}(m,n)}{C_j^{\mp}(m,n)\ \vec{e}_j^{\mp}(m,n)} = \frac{C_i^{\pm}(m,n)e^{\pm\gamma_{mn}z'}}{C_j^{\mp}(m,n)e^{\mp\gamma_{mn}z'}} \quad (12)$$

where the reference plane is located at $x = y = 0$ and $z = z'$.

C. Power Waves at the Device Under Test (DUT)

It is now necessary to define the scattering parameters at the device ports due to incident Floquet harmonics. For the planar geometry as shown in Fig. 1, the device port locations are not terminated in transmission lines with known characteristic impedance. Therefore it is necessary to choose generalized power waves as described by Kurokawa [19]

$$a_k = \frac{V_k + Z_k I_k}{2\sqrt{|\text{Re } Z_k|}} \quad (13)$$

$$b_k = \frac{V_k - Z_k I_k}{2\sqrt{|\text{Re } Z_k|}}. \quad (14)$$

By convenience, the normalizing impedance Z_k at the kth port is chosen to be the input impedance. Thus the scattering parameters as given by (12) are determined with the device ports matched, $V_k = -Z_k I_k$, so that $a_k = 0$.

The scattering parameters between the jth incident Floquet harmonics and kth device ports are then computed via

$$S_{ki} = -I_k\sqrt{|\text{Re } Z_k|} \quad (15)$$

by conveniently choosing $C_j^{\mp}(m,n)e^{\mp\gamma_{mn}z'} = 1$. By reciprocity, the scattering parameters due to excitation at the device ports are found by using the symmetry of the resulting scattering matrix. The input reflection coefficient at the kth device location, S_{kk} is then computed by

$$S_{kk} = \frac{Z_k - Z_k^{*}}{Z_k + Z_k^{*}}. \quad (16)$$

Thus (12), (15), and (16) define the generalized scattering matrix for the periodic array. Note that when the supporting superstrate and substrates materials are lossless, the computed generalized scattering matrix satisfies the usual conditions related to power conservation. The generalized scattering matrix approach will be verified in the next section by measurements in a waveguide simulator.

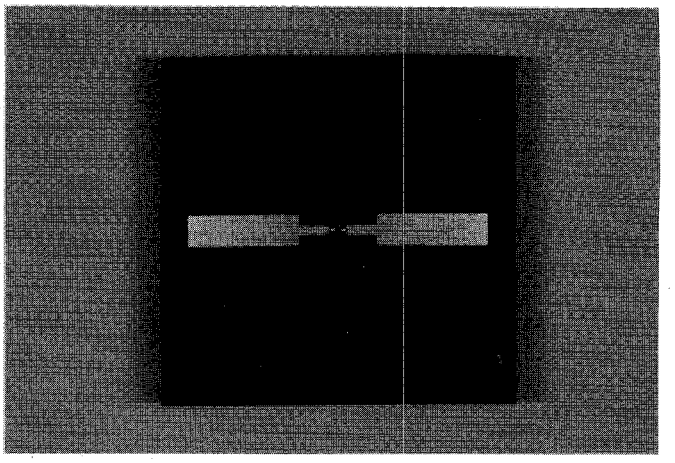

Fig. 3. Unit cell of one-port device for waveguide simulation. The substrate is RT/duroid 5880 with $\epsilon_r = 2.2$ and a thickness of 0.32 cm (0.125 in). The port is terminated with a chip resistor of length 0.1 cm, width 0.05 cm, and height of 0.04 cm.

III. Waveguide Simulation

Fig. 3 shows the one port dipole unit cell to be simulated in a waveguide simulator. The substrate is supported by Rogers RT/duroid 5880, $\epsilon_r = 2.2$, that is 0.32 cm thick. To support two orthogonal modes for two port device measurements, the unit cell was placed in square waveguide. The dimensions of one edge of the square unit cell is 4.74 cm, and the dipole

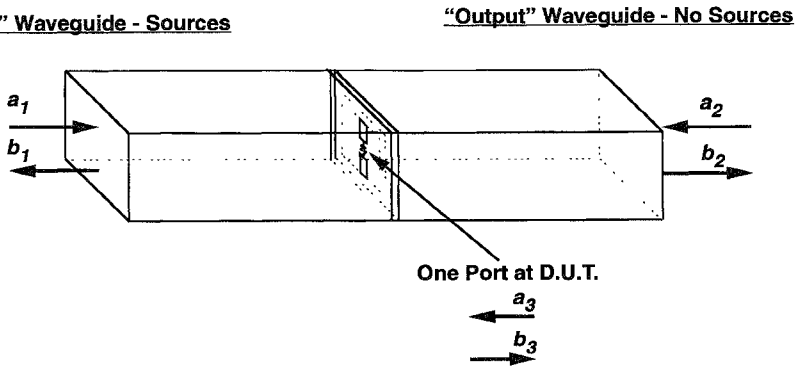

Fig. 4. Waveguide method of one-port S parameter dc-embedding using a single unit cell. Note that $S_{31}, S_{21}, \cdots$ are computed by numerical analysis.

has a length of 4.0 cm and width of 0.44 cm. The dipole is loaded with a chip resistor of length 0.1 cm, width 0.5 cm, and height of 0.04 cm.

Fig. 4 shows a simplified diagram of the one-port device in the waveguide. In this simplified diagram the generalized scattering matrix, S^{num}, computed by the procedure outlined above results in a three-port scattering matrix relating the field quantities at ports 1 and 2, to the power wave representation at the device port of port 3. Upon calibration at the waveguide ports, the computed generalized scattering matrix of S^{num} then forms the embedding network to which the chip resistor is attached. Since the scattering matrix for this embedding network is known, the scattering parameters of the chip resistor load, S^{dut}, can be determined from measurements at waveguide ports 1 and 2. Therefore the approach taken here to verify S^{num} is as follows: the scattering matrix for the embedding network S^{num} will be computed, a known device under test represented by S^{dut} will be attached, the scattering matrix at the external ports of the complete system consisting of S^{num} attached to S^{dut} is measured, S^{dut} is computed from the measured data.

In the more general case which uses a square unit cell the measurement of the two orthogonal TE modes, TE_{01} and TE_{10}, in the square waveguide are required. For measurement of these two orthogonal modes, orthomode junctions become part of the embedding network as shown in Fig. 5. Therefore the generalized scattering matrix for the unit cell, S^{num}, is represented by a five-port generalized scattering matrix for a one-port device, and a six-port generalized scattering matrix for a two-port device. The composite scattering matrix resulting from the combination of S^{num} and S^{dut} with the measured scattering parameters of the orthomodes forms a four-port embedding network. Measurement of the resulting four-port scattering matrix then allows for extraction of S^{dut}.

A. Test Setup Characterization

Addition of the orthomode junctions into the measurement setup requires measurement of the S parameters of these four-port devices. Determination of the S parameters of the orthomodes is complicated by the need to place standards at the square waveguide port that match one of the TE modes, while reflecting the orthogonal mode with known magnitude and phase. This was accomplished by using a stepped transition in one dimension from 4.74 cm to 3.27 cm, and then from 3.27 cm to rectangular waveguide of 2.21 cm by 4.74 cm, which only supports one dominant TE mode. A mode-matching solution was used to calculate the magnitude and phase of the stepped transition so that it could be used as a standard in determination of the S parameters of the orthomode junctions.

In order for the relatively narrow band stepped transitions to exhibit greater than 20 dB return loss, and to avoid introduction of the higher order TE_{11} and TM_{11} modes, it was necessary to limit the measurement range from 4.0 GHz to 4.4 GHz. Note that the addition of the orthomodes creates a source of uncalibrated error in the measurement system, which is calibrated in rectangular waveguide. Assessment of errors due to the presence of the orthomodes was done by connecting two "identical" orthomodes so that their square waveguide ports are together. The external ports presented then allow for a four port measurement in rectangular waveguide. Thus the perfect "thru" junction between the two orthomodes can be de-embedded. This measurement indicated a maximum of 8% error in magnitude of one propagating mode, and 3% error in the magnitude of the orthogonal square waveguide mode with phase error less than 2.2 degrees for both modes.

The use of square waveguide for simulation of a periodic array requires the solution of the periodic array problem for the two Floquet modes composing the TE_{01} mode. These plane waves are incident at an angle θ which varies from 46 to 52 degrees over the frequency range of the measurement. This large angle of incidence results in additional reflection of the $m = -1$ Floquet harmonic, which must be properly combined with the two original exciting modes when forming S^{num}. In order to satisfy the boundary conditions of the square waveguide, a rotation of $\phi = 90$ degrees then computes the parameters for the TE_{10} mode. Thus a ten-port representation of S^{num} using Floquet modes is reduced to a six-port scattering matrix for waveguide simulation with a two-port device.

The square waveguide simulation of the grid amplifier used here forces plane wave solutions that satisfy the boundary conditions of the waveguide. Therefore it must be realized that only in order to compare with waveguide measurement is this behavior being forced on the solutions. It is noted that waveguide simulation of a single unit cell is only equivalent to an infinitely periodic grid amplifier when the periodic amplifier

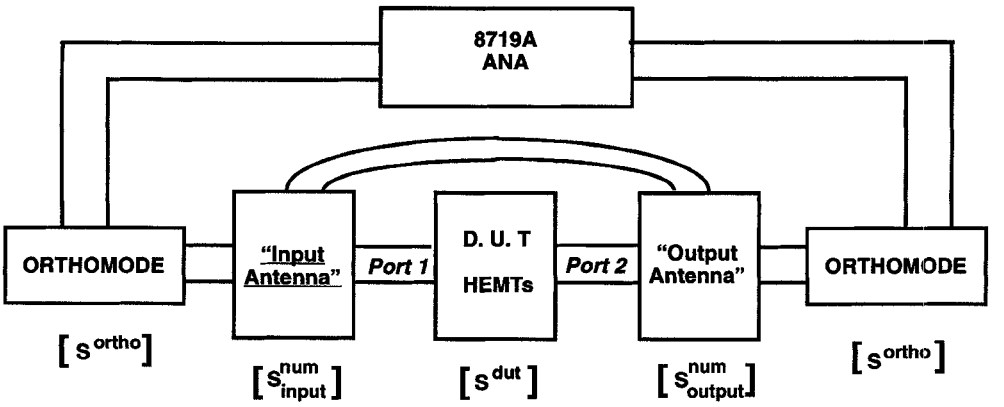

Fig. 5. Waveguide method of two-port S parameter de-embedding using a single unit cell and two orthomode junctions to verify S^{num} and measure S^{dut}.

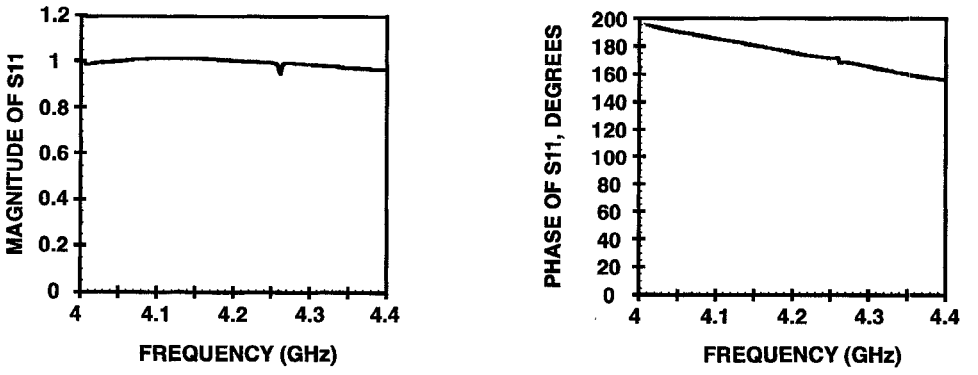

Fig. 6. De-embedded S^{dut} parameters using the unit cell shown in Fig. 3 when the load is a conducting patch, (a) measured S_{11} magnitude and (b) measured S_{11} phase.

is operating in modes properly imaged by the waveguide walls. It is noted that the infinitely periodic grid amplifier is not limited to this subset of its possible modes of operation, nor is the generalized scattering matrix approach.

The use of Floquet modes allows the approach here to be applied to arbitrary angles of incidence, in addition to those that satisfy the waveguide boundary conditions. This is evident in the inclusion of two plane waves to properly form the TE_{01} mode as described above. In practice we expect the array to be excited by a single plane wave at an arbitrary angle θ, which need not be representable by a waveguide simulator, and would choose the Floquet modes for this angle of incidence. Therefore the generalized scattering matrix could also be applied to grid oscillators operating in a mode that cannot be simulated using a single unit cell in a waveguide. For grid amplifier design this method is also applicable to a grid suffering from common-mode oscillations [20].

B. Results for a One-Port DUT

Fig. 6 shows the results of de-embedding the S^{dut} parameters of the unit cell shown in Fig. 3 when the load is replaced by a conducting patch. The de-embedded S^{dut} parameter shown is normalized to the antenna input impedance. The superstrate layer for this unit cell consists of an air layer with a thickness of 1 cm. The inclusion of the air superstrate layer allows the generalized scattering matrix for the array to be properly referenced to the interface of the support fixture for the unit cell, and the face of the orthomode junction. The support fixture used consisted of a square waveguide section of length 1.32 cm in which the unit cell was press fitted. This allowed for removal and replacement of the device under test.

Fig. 7 shows the de-embedded S^{dut} parameter for the unit cell shown in Fig. 3 when it is loaded with a 51 Ω chip resistor. The theoretical curve is computed by using the computed input impedance, Z_{in}, which is the normalizing impedance. The frequency dependence of the theoretical curves is due to the slight variation in the input impedance which varies from $(164.8 - j8.2)\ \Omega$ to $(178.8 + j6.1)\ \Omega$ from 4.0 to 4.4 GHz. The maximum error in the measured magnitude of the device S parameter is 8.6%.

The load impedance magnitude and phase for the one-port device can be calculated since the normalizing impedance, the input impedance at the device port Z_{in}, is known

$$Z_{\text{load}} = \frac{S^{\text{dut}} Z_{in} + Z_{in}}{1 - S^{\text{dut}}}. \tag{17}$$

The nonlinear nature of this conversion may increase or decrease the error in the measured S parameter S^{dut}, but puts the results in a more readable form. Fig. 8 shows the measured load impedance magnitude and phase as computed from (17). The measured load magnitude is in error by approximately 8.4%. As expected the relative error when represented by

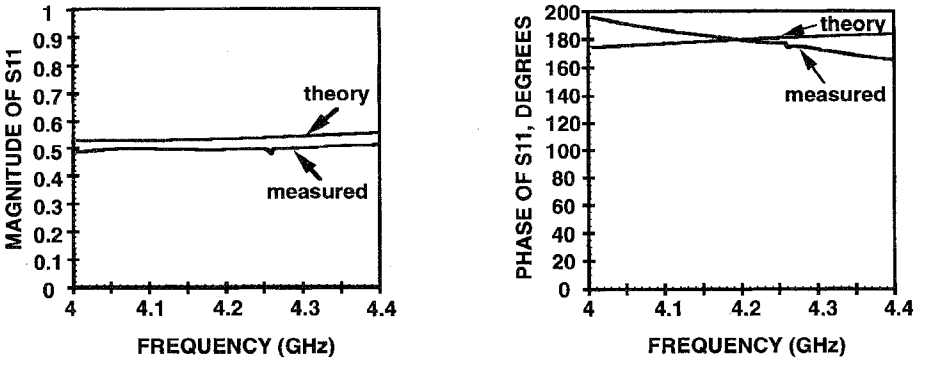

(a) (b)

Fig. 7. De-embedded S^{dut} parameters using the unit cell shown in Fig. 3 when the load is a 51-ohm chip resistor, (a) measured S_{11} magnitude and (b) measured S_{11} phase.

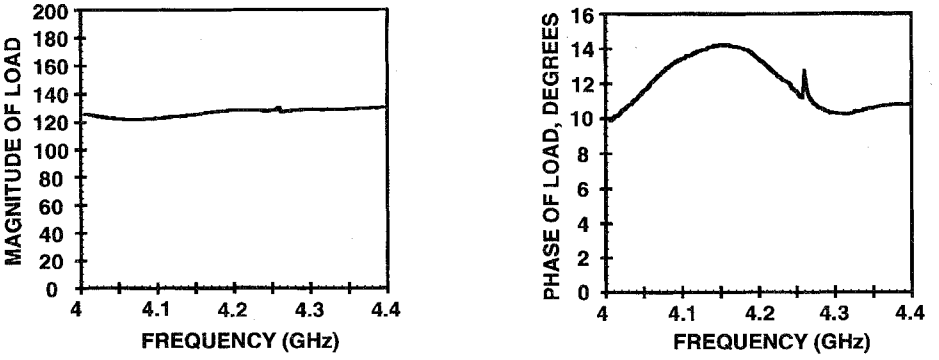

(a) (b)

Fig. 8. De-embedded load impedance of the unit cell shown in Fig. 3 when the load is a 120–ohm chip resistor, (a) measured load magnitude and (b) measured load phase.

(17) was minimal when the loading chip resistor was more closely matched to the input impedance presented at the device. Although it was not done here, incorporation of error correction terms into the measurement system would alleviate these problems.

It is appropriate to make some comment about the phase gradients shown in Figs. 6(b) and 7(b). Some success in minimizing the phase gradients was experienced by changing the reference plane for the 0.32 cm thick substrate in the square waveguide support fixture of length 1.32 cm. This indicates that the phase gradient may be representative of a small length change in the measurement system caused by insertion and removal of the support fixture, or movement of the test piece in the support fixture.

Also measurement spikes are shown in all measured curves near 4.25 GHz, as can be seen in Fig. 8(b). The origin of the spikes is related to the phase change of the S parameter for the orthomode junction that describes the relationship between a square waveguide port and its strongly coupled rectangular port. At the frequency of 4.25 GHz there is a 180-degree phase change in this orthomode scattering parameter. Since the two orthomodes are not truly identical, this phase change occurs at slightly different frequencies. Again it is believed that proper error correction terms could remove this error. An appropriate calibration piece for determination of the error terms would be the unit cell shown in Fig. 3 when the load is the conducting patch. The scattering matrix for this calibration piece would be computed by the methods described here.

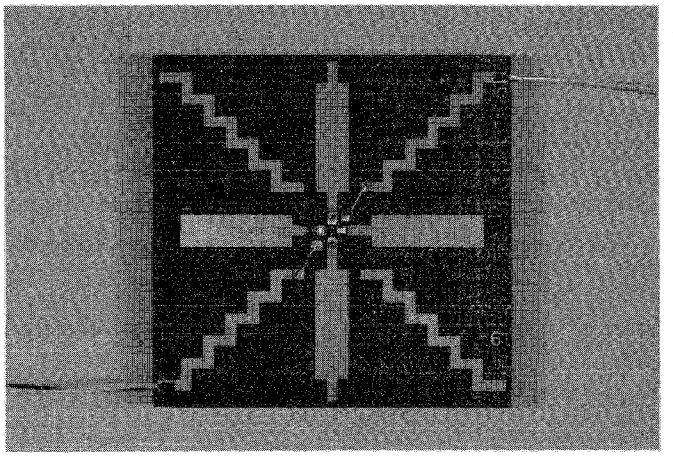

Fig. 9. Unit cell of two-port device for waveguide simulation. The substrate is RT/duroid 5880 with $\epsilon_r = 2.2$ with a thickness of 0.32 cm $(0.125in)$. The port is terminated with a differential pair HEMT designed and fabricated at JPL.

Before moving to results for two-port devices it is noted that measured transmitted and reflected parameters of the loaded unit cell, such as those depicted by S_{21} and in S_{12} in Fig. 4, were also measured and compared to theoretical results. These four-port parameters were, in general, of similar accuracy

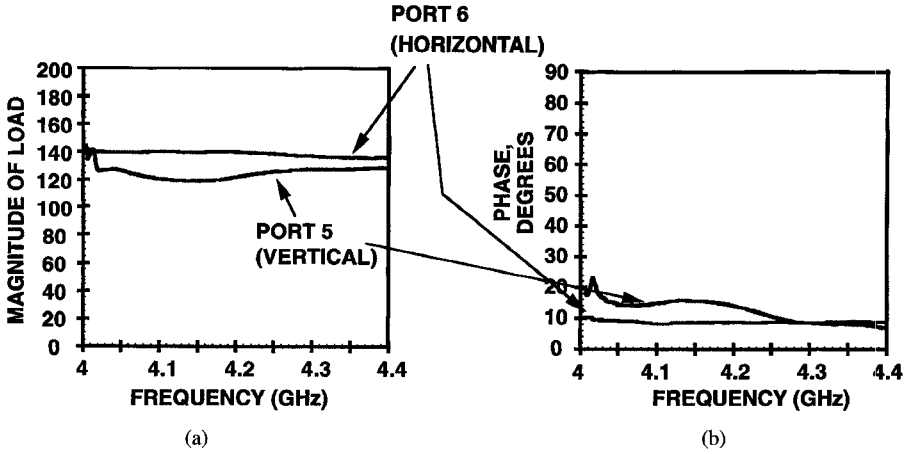

Fig. 10. De-embedded two-port S^{dut}: load impedances of the unit cell shown in Fig. 9 when the loads are two 120-ohm chip resistors, (a) measured load magnitude and (b) measured load phase.

to the load de-embedding results presented. This provided another method of verifying a composite scattering matrix formed from the combination of the generalized scattering parameters for the periodic array, S^{num}, and the parameters of the device, S^{dut}. A final check on this composite scattering matrix results from including the chip resistor directly in the computation of S^{num} through the surface impedance in (1).

C. Results for a Two-Port DUT

Fig. 9 shows the two-port unit cell used for waveguide simulation. The substrate and individual dipole dimensions are the same as the single dipole shown in Fig. 3. By separating orthogonal chip resistors by a thin layer of polyimide, each individual dipole was loaded independently with no connection to the other device. In this configuration equation (17) can be used to de-embed the load impedance values, the chip resistors, from the measured data. Fig. 10 shows the measured results when two 120 Ω chip resistors are used. The average error on the vertical loaded port, port 5, is 4.4% while the average error on the horizontal port, port 6, is 15.8%. This is more error than expected due to a worst case linear summation of the two polarizations of the orthomodes, 11%. The maximum phase angle measured was 24 degrees.

D. Results for a Differential Pair HEMT Two-Port DUT

Since it is difficult to measure the differential pairs often used in grid amplifiers [3]–[5] when operating in a balanced mode, waveguide simulation of a single unit cell provides a means of measuring these parameters. The unit cell configuration shown in Fig. 9 was used to measure a differential pair HEMT wire bonded in the configuration shown in Fig. 1. Upon measurement of the four-port scattering matrix at the external rectangular waveguide ports of the two orthomode junctions, the two-port S^{dut} parameters of the differential HEMT pair were extracted for different bias levels.

The monolithic differential pair, shown in Fig. 1, consists of two 0.15 micron, pseudomorphic HEMT's along with various passive circuitry. The devices are arranged with common sources. The source bias pads are connected to the device

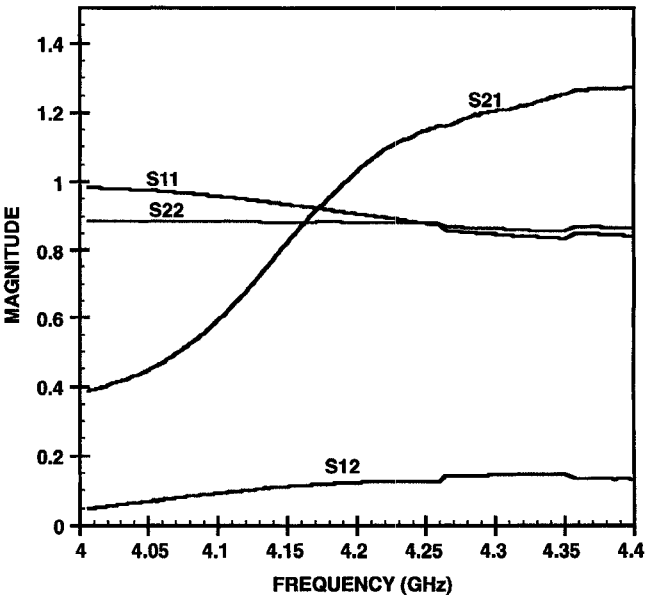

Fig. 11. Magnitude of de-embedded device S^{dut} parameters, normalized to 50 ohms, when the unit cell shown in Fig. 9 is loaded with a differential pair HEMT biased at 5 V, 8.0 mA.

sources through 50 Ω resistors in order to suppress common-mode oscillations [4]. This resistance will contribute to the dc power consumption of the chip, but since the sources themselves are connected together, the resistance does not degrade the device gain. Gates are connected to ground through a higher value resistor for simplicity, although this approach adversely affects the gain and provides no means for adjusting the gate bias.

Fig. 11 shows the de-embedded two-port S^{dut} parameters of the differential pair HEMT. The devices are biased with a drain bias of 5 V and 8 mA. To put the generalized scattering parameters in a more standard form, Fig. 11 shows scattering parameters normalized to 50 ohms. Note the large mis-match of the devices to both input and output ports, as represented by S_{11} (gates) and S_{22} (drains), for this normalizing impedance. Even with the mis-matches on input and output the necessary

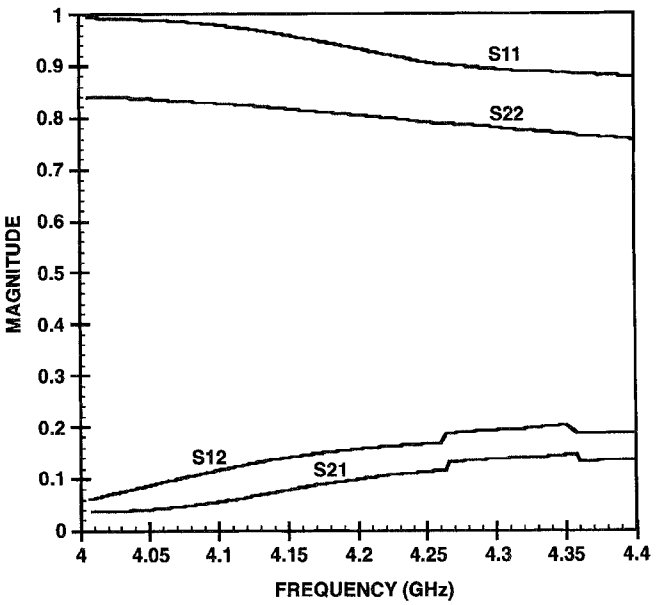

Fig. 12. Magnitude of de-embedded device S^{dut} parameters, normalized to 50 ohms, when the unit cell shown in Fig. 9 is loaded with a differential pair HEMT biased at 0 V.

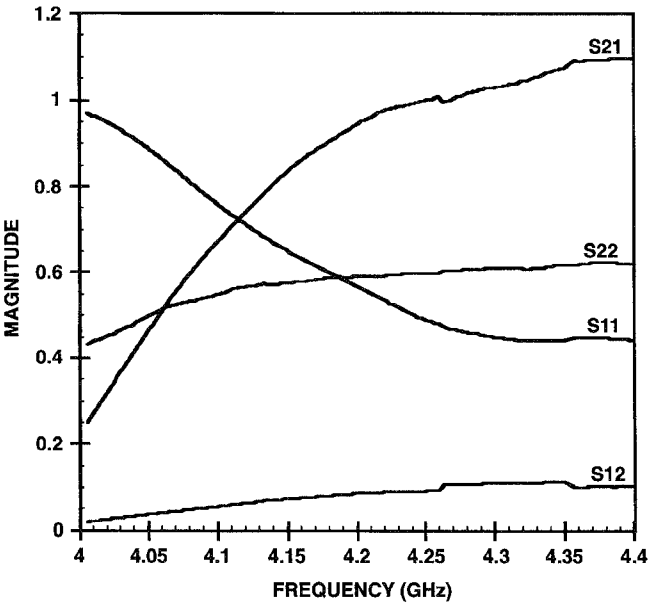

Fig. 13 De-embedded device S^{dut} parameters, normalized to input impedances, when the unit cell shown in Fig. 9 is loaded with a differential pair HEMT biased at 5 V, 8.0 mA.

conditions for stability

$$|S_{11}| < 1, \quad |S_{22}| < 1 \tag{18}$$

are satisfied. Fig. 12 shows the scattering parameters normalized to 50 ohms when the drain bias becomes 0 V.

Fig. 13 shows the magnitude of the generalized scattering parameters as computed, where the normalizing impedances are the input impedances at the ports. This corresponds to the actual device loading presented by the grid during the waveguide measurement. The result is a more desirable match to the device at higher frequencies as shown. And as the input match improves, the transducer power gain, $S21$, increases until the maximum of 0.8 dB is reached at 4.4 GHz.

The generalized scattering matrix for the unit cell S^{num} is represented by a six-port generalized scattering matrix for this two-port device. The coupling between port 5 of the vertical dipole and port 6 of the horizontal dipole is <-40 dB. This coupling represents the feedback through the embedding array from the output of the devices to the input, and was minimized by the symmetric geometry chosen.

IV. Conclusion

A generalized scattering matrix for modeling of grid amplifier and oscillator arrays has been developed and verified experimentally. The method incorporates a generalized scattering matrix representation for the embedding periodic array, where Floquet harmonics represent ports of the array. These additional ports are combined with power wave representations at the device ports, which are in the plane of the array.

The presence of the device ports allows the scattering matrix representation for the embedding array to be combined with a scattering matrix for the device. Thus standard scattering matrix design methods and approaches are valid for grid amplifier design. To verify this, the computed generalized scattering matrix for the embedding array, S^{num}, was used to de-embed the scattering parameters of known chip resistors. Experimentally this involved using a waveguide simulation of one unit cell, and combining the scattering matrices of two orthomode junctions with the scattering matrix of the embedding array, S^{num}. With the scattering matrix between the rectangular waveguide ports of the orthomodes and the device ports in the unit cell then known, conventional de-embedding techniques were used to determine the chip resistor values, S^{dut}. Results for loaded dipoles with one-port and two-port devices were presented. Scattering parameters of a differential pair amplifier, operating in a balanced mode, were measured using a single unit cell of a grid amplifier.

The use of Floquet harmonics avoids magnetic and electric wall assumptions. Use of TE and TM Floquet modes allows the orthogonal polarizations of the grid amplifier to be defined as input and output ports in the scattering matrix. If a grid amplifier, such as the one shown in Fig. 1, is excited by a horizontal polarization the output is predominantly polarized in the vertical direction. But, the presence of bias lines causes coupling between input and output polarizations. Using the generalized scattering matrix, this coupling was computed for the geometry shown in Fig. 9. In addition the stability conditions at the device ports were examined for this geometry.

The waveguide simulator environment, which specified non-normal angles of incidence, demonstrates the flexibility of this approach for analyzing periodic grid amplifier and grid oscillator arrays. Although not demonstrated here, the Floquet mode representation allows for the combination of polarizers and other periodic structures commonly used in quasi-optical setups by cascading of scattering matrices [9]. Furthermore, the generalized scattering matrix representation lends itself to

examination of the input and output stability circles of such a quasi-optical system.

ACKNOWLEDGMENT

The authors would like to thank R. Perez for his measurement assistance, and G. Chinn for analyzing the stepped transitions needed to measure the S parameters of the orthomode junctions. Discussions with D. Rutledge and his research group, including M. Kim and A. Moussessian, are similarly acknowledged.

REFERENCES

[1] Z. B. Popović, R. M. Weikle II, M. Kim, and D. B. Rutledge "A 100 MESFET planar grid oscillator," *IEEE Trans. Microwave Theory Tech.*, vol. 39, no. 2, pp. 193–200, Feb. 1991.

[2] R. M. Weikle II, M. Kim, J. B. Hacker, M. P. De Lisio, and D. B. Rutledge "Planar MESFET grid oscillators using gate feedback," *IEEE Trans. Microwave Theory Tech.*, vol. 40, no. 11, pp. 1997–2003, Nov. 1992.

[3] R. M. Weikle II, M. Kim, J. B. Hacker, M. P. De Lisio, Z. B. Popović, and D. B. Rutledge "Transistor oscillator and amplifier grids," *Proc. IEEE*, vol. 80, pp. 1800–1809, Nov. 1992.

[4] M. Kim, J. J. Rosenberg, R. Peter Smith, R. M. Weikle, II, J. B. Hacker, M. P. DeLisio, and D. B. Rutledge, "A grid amplifier," *IEEE Microwave Guided Wave Lett.*, vol. 1, no. 11, pp. 322–324, Nov. 1991.

[5] M. Kim, E. A. Sovero, J. B. Hacker, M. P. De Lisio, J. C. Chiao, S. J. Li, D. R. Gagnon, J. J. Rosenberg, and D. B. Rutledge "A 100-element HBT grid amplifier," *IEEE Trans. Microwave Theory Tech.*, vol. 41, no. 10, pp. 1762–1771, Oct. 1993.

[6] S. C. Bundy and Z. B. Popović, "A generalized analysis for grid oscillator design," *IEEE Trans. Microwave Theory Tech.*, vol. 42, no. 12, pp. 2486–2491, Dec. 1994.

[7] ——, "Analysis of cascaded quasi-optical grids," in *IEEE MTT-S Symp. Dig.*, vol. 2, May 1995, pp. 601–604.

[8] M. Guglielmi and A. A. Oliner, "Multimode network description of a planar periodic metal-strip grating at a dielectric interface - part I: rigorous network formulations," *IEEE Trans. Microwave Theory Tech.*, vol. 37, no. 3, pp. 534–541 Mar. 1989.

[9] T. A. Cwik and R. Mittra, "The cascade connection of planar periodic surfaces and lossy dielectric layers to form an arbitrary periodic screen," *IEEE Trans. Antennas Propagat.*, vol. AP-35, no. 12, pp. 1397–1405, Dec. 1987.

[10] R. C. Hall, R. Mittra, and K. M. Mitzner, "Analysis of multilayered periodic structures using generalized scattering matrix theory" *IEEE Trans. Antennas Propagat.*, vol. 36, no. 4, pp. 511–517, Apr. 1988.

[11] N. K. Das and D. M. Pozar, "Multiport scattering analysis of general multilayered printed antennas fed by multiple feed ports: part I—theory," *IEEE Trans. Antennas Propagat.*, vol. 40, no. 5, pp. 469–481, May 1992.

[12] P. C. Sharma and K. C. Gupta, "A generalized method for de-embedding of multiport networks," *IEEE Trans. Instrum. Meas.*, vol. IM-30, pp. 305–307, Dec. 1981.

[13] K. M. Mitzner, "Effective boundary conditions for reflection and transmission by and absorbing shell of arbitrary shape," *IEEE Trans. Antennas Propagat.*, vol. AP-16, no. 6, pp. 706–712, Nov. 1968.

[14] C. H. Tsao and R. Mittra, "Spectral-domain analysis of frequency selective surfaces comprised of periodic arrays of cross dipoles and Jerusalem crosses," *IEEE Trans. Antennas Propagat.*, vol. AP-32, no. 5, pp. 478–486, May 1984.

[15] T. Itoh, "Spectral domain immitance approach for dispersion characteristics of generalized printed transmission lines," *IEEE Trans. Microwave Theory Tech.*, vol. MTT-28, no. 7, pp. 733–736, July 1980.

[16] C. H. Chan and R. Mittra, "On the analysis of frequency selective surfaces using subdomain basis functions," *IEEE Trans. Antennas Propagat.*, vol. 38, no. 1, pp. 40–50, Jan. 1990.

[17] L. Epp, C. H. Chan, and R. Mittra, "The study of FSS surfaces with varying surface impedance and lumped elements," *Abstracts of the 1989 IEEE AP-S Int. Symp.*, San Jose, CA, vol. 2, pp. 1056–1059, June 1989.

[18] V. Galindo, N. Amitay, and C. P. Wu, *Theory And Analysis of Phased Array Antennas.* New York: Wiley-Interscience, 1972.

[19] K. Kurokawa, "Power waves and the scattering matrix," *IEEE Trans. Microwave Theory Tech.*, vol. MTT-13, pp. 194–202, Mar. 1965.

[20] J. S. H. Schoenberg, S. C. Bundy, and Z. B. Popović, "Two-level power combining using a lens amplifier," *IEEE Trans. Microwave Theory Tech.*, vol. 42, no. 12, pp. 2480–2485, Dec. 1994.

[21] R. A. York, P. Liao, and J. J. Lynch, "Oscillator array dynamics with broadband N-port coupling networks," *IEEE Trans. Microwave Theory Tech.*, vol. 42, no. 11, pp. 2040–2045, Nov. 1994.

[22] J. Fang and D. Xeu, "Numerical errors in the computation of impedances by FDTD method and ways to eliminate them," *IEEE Microwave and Guided Wave Lett.*, vol. 5, no. 1, pp. 6–8, Jan. 1991.

[23] C.-M. Liu, E. A. Sovero, M. P. De Lisio, A. Moussessian, J. J. Rosenberg, and D. B. Rutledge, "Gain and stability models for HBT grid amplifiers," *Abstracts 1995 IEEE AP-S Int. Symp.*, Newport Beach, CA, vol. 2, pp. 1292–1295, June 1995.

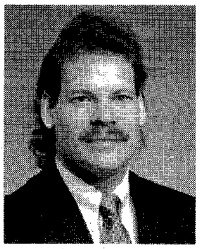

Larry W. Epp (S'82–M'90) was born in Lincoln, NE, in 1962. In 1984 he received the B.S.E.E. degree from Bradley University, Peoria, IL, in 1984. He received the M.S. and Ph. D. degrees in electrical engineering from the University of Illinois in 1986 and 1990, respectively. He received the Ph.D. degree from the Electromagnetic Communication Laboratory, University of Illinois,

He worked briefly for TRW in Redondo Beach, and is now with the Jet Propulsion Laboratory in Pasadena, CA where his tasks include designing and building dichroic plates and FSS for the NASA/JPL Deep Space Network, and developing rectenna arrays. His research interests include the development of grid amplifiers for transmitter and instrument needs on the next generation of small and lightweight spacecraft, hybrid finite element methods, and numerical techniques.

R. Peter Smith (M'87) received the B.S. degree in physics from Bates College in 1977 and the M.S. and Ph. D. degrees, also in physics, from Brown University in 1982 and 1986, respectively.

From 1977 until 1979 he worked at Sunsearch, Inc., and from 1986-1990 he worked at the GE Electronics Laboratory in Syracuse, NY, developing power FET's and HEMT's. He is currently working in the Microdevices Laboratory at the Jet Propulsion Laboratory. Areas of research include advanced processing techniques for III-V devices, sub-millimeter device and circuit development, and wide-bandgap power devices.